Understanding the chemistry of the rocks at Jezero crater, Mars, through the combined use of SuperCam spectroscopic and optical techniques

J. M. Madariaga[1*], R. C. Wiens[2], G. Arana[1], V. Sautter[3], K. Benzerara[3], A. Udry[4], O. Beyssac[3], L. Mandon[5], O. Gasnault[6], J.R. Johnson[7], A. M. Ollila[2], K. Castro[1], A. Cousin[6], S. Maurice[6], S. Clegg[2], R. B. Anderson[8], T. Bosak[9], P. Beck[10], T. Fouchet[5], S. Shkolyar[11], E. Cloutis[12], C. Quantin-Nataf[13], I. Torre-Fdez[1], C. Royer[5], C. Legett[2], P. Pilleri[6], and the SuperCam team

[1]University of the Basque Country (UPV/EHU), Bilbao, Spain; [2]Los Alamos National Laboratory, Los Alamos, NM, USA; [3]IMPMC, Museum National d'Histoire Naturelle, CNRS, Sorbonne Université, Paris, France; [4]University of Nevada, Las Vegas, NV, USA; [5]LESIA, Observatoire de Paris, Université PSL, CNRS, Sorbonne Université, Meudon, France; [6]IRAP, CNRS, Université de Toulouse, UPS-OMP, Toulouse, France; [7]John Hopkins University Applied Physics Laboratory, Laurel, MD, USA; [8]U.S. Geological Survey, Flagstaff, AZ, USA; [9]Dept. Earth, Atmospheric and Planetary Science, MIT, MA, USA; [10]Université Grenoble-Alpes, CNRS, IPAG, UMR 5274, Grenoble, France; [11] NASA Goddard Space Flight Center, MD, USA; [12]University of Winnipeg, Winnipeg, Canada; [13]Université de Lyon, LGL-TPE UCBL, ENSL, CNRS Lyon, France; (*) juanmanuel.madariaga@ehu.eus

INTRODUCTION

The SuperCam instrument onboard Perseverance rover has remote imaging (RMI), VISIR, LIBS, Raman and Time-Resolved Luminescence (TRL) capabilities. Once the post-landing tests on all elements and spectrometers of SuperCam were completed, the science activities started with the analysis of rocks, pebbles, and soils, first at the Octavia E. Butler (OEB) landing site and then in the Crater Floor Fractured Rough (Cf-fr) unit (Sol <170), in the Artuby ridge (170≤Sol≤201), and currently in the Seitah unit (Sol >201), as depicted in Figure 1 for the Sols until Conjunction.

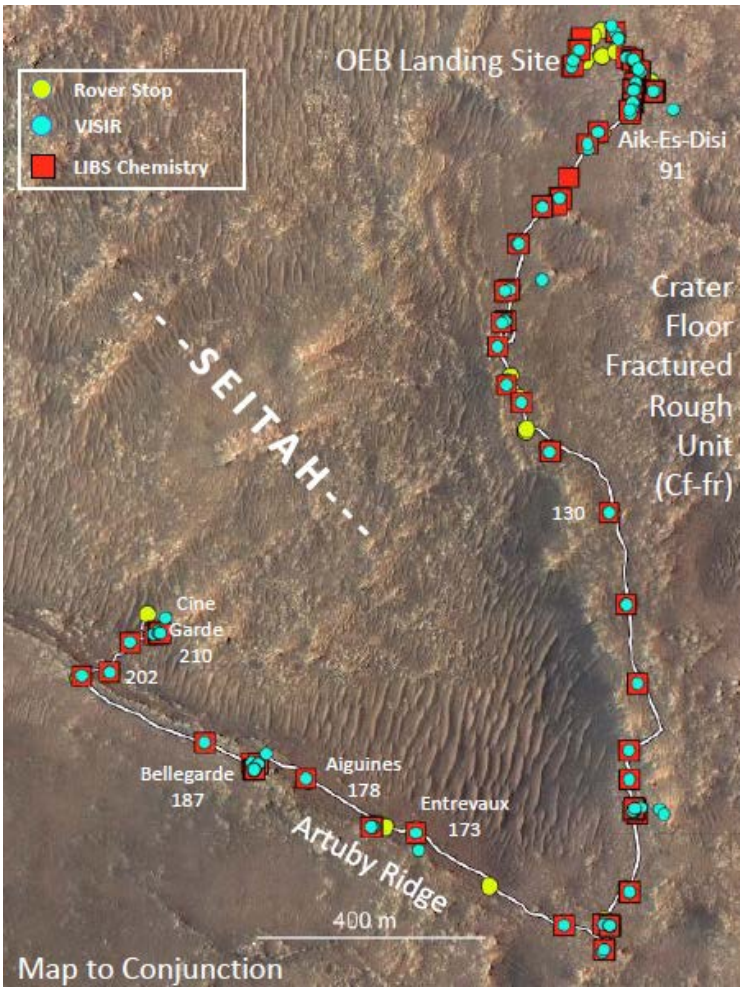

Figure 1.- Traverse of the Perseverance rover indicating the sites where SuperCam performed science activities until Conjunction. Since then it has collected two samples of Seitah.

IMAGE AND SPECTROSCOPIC OBSERVATIONS

RMI images of the rocks at the OEB landing site and the Cf-fr unit, both High-Standing (Cf-Fr Hi) and Low-standing (Cf-fr Lo) rocks (Figure 2), have revealed important granular texture diversities. VISIR raster point observations have revealed important differences in the 2.10-2.50 µm infrared range (metal-hydroxides); many include water features at 1.40±0.04 and 1.92±0.02 µm [1] suggesting the presence of alteration minerals. LIBS observations on the same points analyzed by VISIR revealed important differences in the concentrations of major elements, suggesting mineral grain sizes larger than the laser beam (300-500 µm); moreover, the sum of the 8 major elements (%SiO_2, %TiO_2, %Al_2O_3, %FeOT, %MgO, %CaO, %Na_2O, and %K_2O) quantified from LIBS spectra never reached 100%, suggesting the presence of alteration phases.

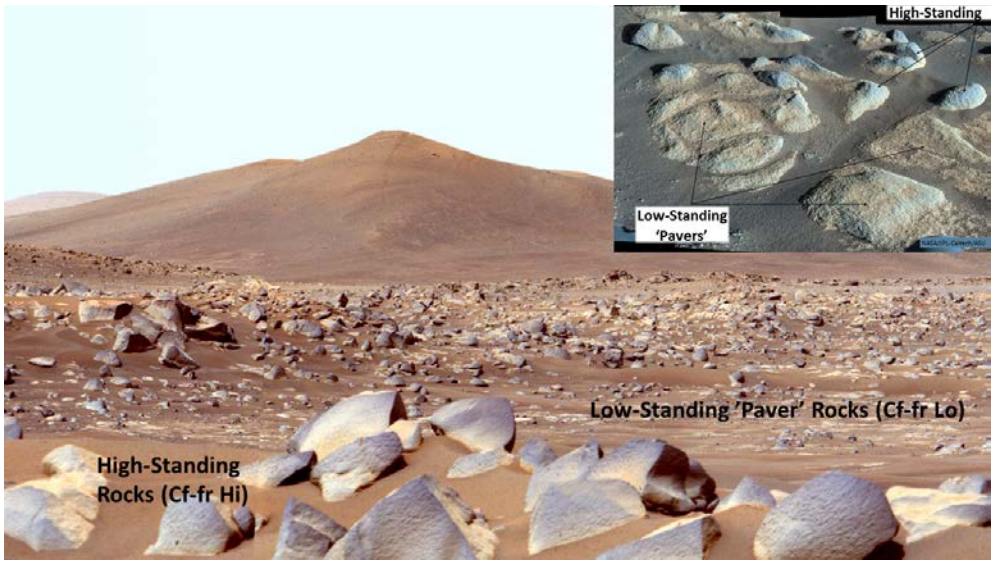

Figure 2.- High-Standing (Cf-Fr Hi) and Low-standing (Cf-fr Lo) rocks at the Crater Floor Fracture Rough unit. The Cf-fr Hi are darker rocks while the Cf-fr Lo are paver rocks.

LIBS elemental compositions of rocks at the OEB landing site and the Cf-Fr unit are consistent with pyroxenes, feldspars, and more often feldspar-like glass, often enriched in silica. Olivine compositions [1, 2] have been observed so far in LIBS data (up to Sol 140) exclusively in rounded regolith pebbles. They were not observed in the Cf-fr rocks themselves, which are MgO-poor compared to regolith and are consistent with FeO bearing pyroxenes (e.g., hedenbergite, ferrosilite). Figure 3 shows the dispersion obtained from those rock targets, with observations close to andesine and enstatite endmembers and intermediate situations close to diopside (the black points belong to the pyroxenes and olivine present in the calibration target of SuperCam).

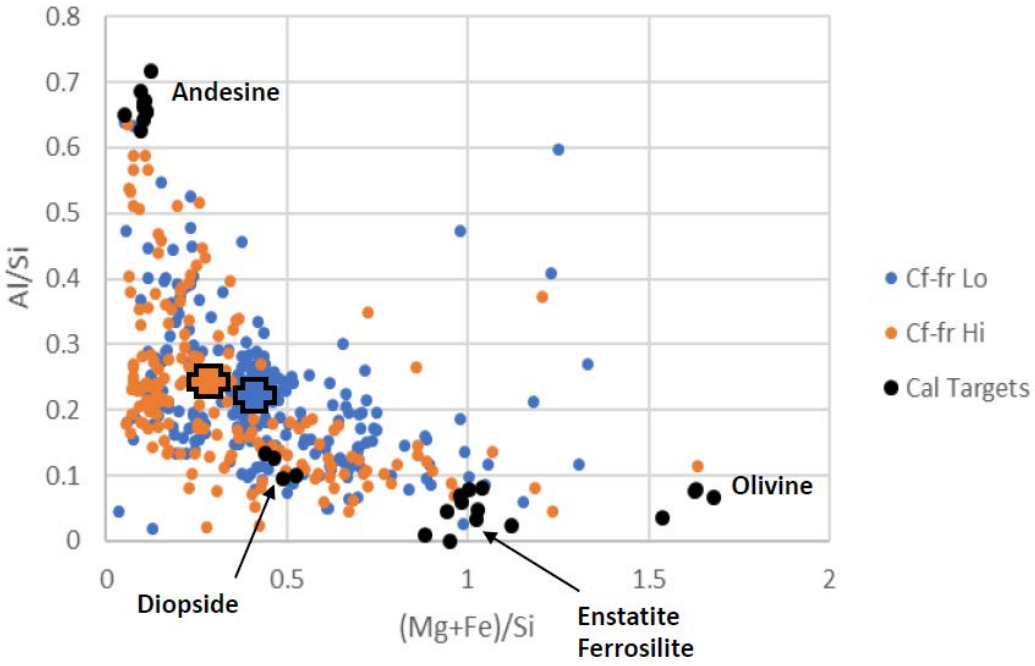

Figure 3.- Diversity of the Cf-Fr Hi and Cf-fr Lo rocks in comparison with the pyroxene-olivine samples included in the calibration target of SuperCam. Crosses are the mean value for each rock type.

A 3x3 LIBS and VISIR raster (9x9 mm) acquired on the Tostid_tsaadah low-standing rock on sol 90 exemplifies these findings. Figure 4 shows the geologic context of rock containing the Tostid_tsaadah target (NavCam image), and the proximity (RMI image) and detail of the 9 points of the raster. Table 1 summarizes the %MeO values, with their uncertainties (standard deviations of 25 spectra at each observation point), for the 9 observations on this target.

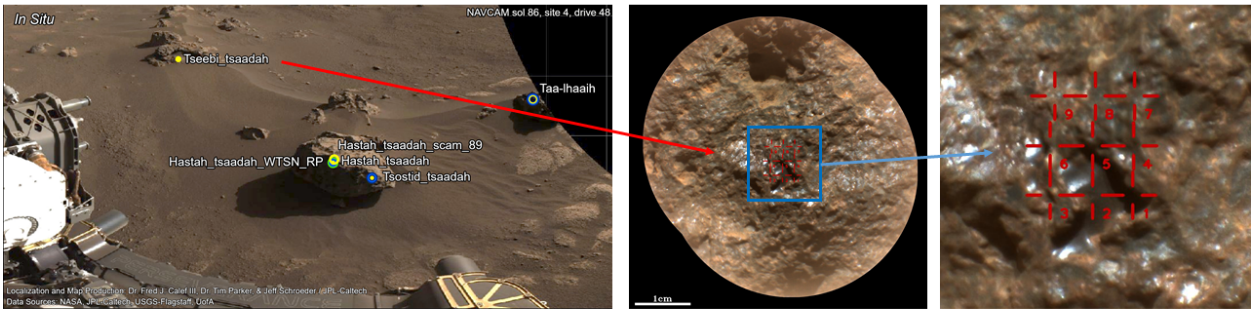

Figure 4.- Long distance, proximity and near microscopic detail of the Tostid_tsaadah target

Table 1.- Percent of Metal-Oxide units for concentrations and standard deviation values of Tostid_tsaadah low-standing rock, Sol 90

Point	SiO2	SiO_2 stdev	TiO_2	TiO_2 stdev	Al_2O_3	Al_2O_3 stdev	FeOT	FeOT stdev	MgO	MgO stdev	CaO	CaO tdev	Na_2O	Na_2O stdev	K_2O	K_2O stdev	Total
1	1.07	1.85	0.06	0.01	1.61	1.62	80.56	3.05	2.52	0.93	0.66	0.50	1.02	0.11	0.51	0.63	88.01
2	3.98	1.85	0.07	0.01	2.12	0.83	82.85	2.68	3.66	0.92	1.24	0.71	1.32	0.07	0.00	0.08	95.24
3	26.63	8.54	0.07	0.02	3.79	1.57	49.15	13.27	2.72	0.85	2.03	0.61	1.66	0.18	1.00	0.57	87.05
4	51.13	1.81	0.11	0.01	3.08	1.01	40.06	5.12	0.86	0.48	1.57	0.39	1.64	0.32	0.30	0.29	98.75
5	62.50	1.29	0.18	0.04	12.30	0.67	2.42	0.87	0.69	0.16	1.19	0.28	4.31	0.28	4.51	0.48	88.10
6	45.04	3.13	0.03	0.01	5.98	1.11	35.73	4.93	3.22	1.46	1.86	0.54	3.96	0.26	1.26	0.52	97.08
7	23.87	2.90	1.96	0.09	4.21	1.58	27.79	7.33	2.54	1.09	3.46	0.45	1.90	0.34	0.48	0.51	66.21
8	46.20	5.07	0.52	0.06	1.89	1.18	61.94	7.19	1.62	0.67	1.26	0.66	1.41	0.11	0.42	0.63	115.26
9	51.46	3.06	0.46	0.20	7.03	1.15	13.36	5.55	3.13	0.86	4.17	1.66	3.39	0.36	1.63	0.45	84.63

The dark L-shaped filled void, sampled by points 1 and 2, shows high H signal in LIBS, together with the highest concentration of Fe and the lowest of Si, and the VISIR spectra is consistent with ferrihydrite [1]. Point 5 contains abundant silica and alkali elements, with a molar ratio of Al/(Na+K) close to 1, consistent with albite in an amount of 64% of the total mass; the excess of silica could be consistent with dacitic glass composition. Point 7 has TiO_2 content consistent with ilmenite (the calibration underestimates Ti at high abundances).

The rocks analyzed along Artuby ridge (Fig. 1) started to show clear olivine signatures in the VISIR spectra, as depicted by the slope of the spectra in the 1.3-1.8 µm range. This was more evident when the rover left Artuby and started the Seitah campaign, as it can be observed in Figure 5 where the slope, in the 1.3-1.8 µm range, of the VISIR spectra collected from the beginning of the mission is plotted against the Sol numbers.

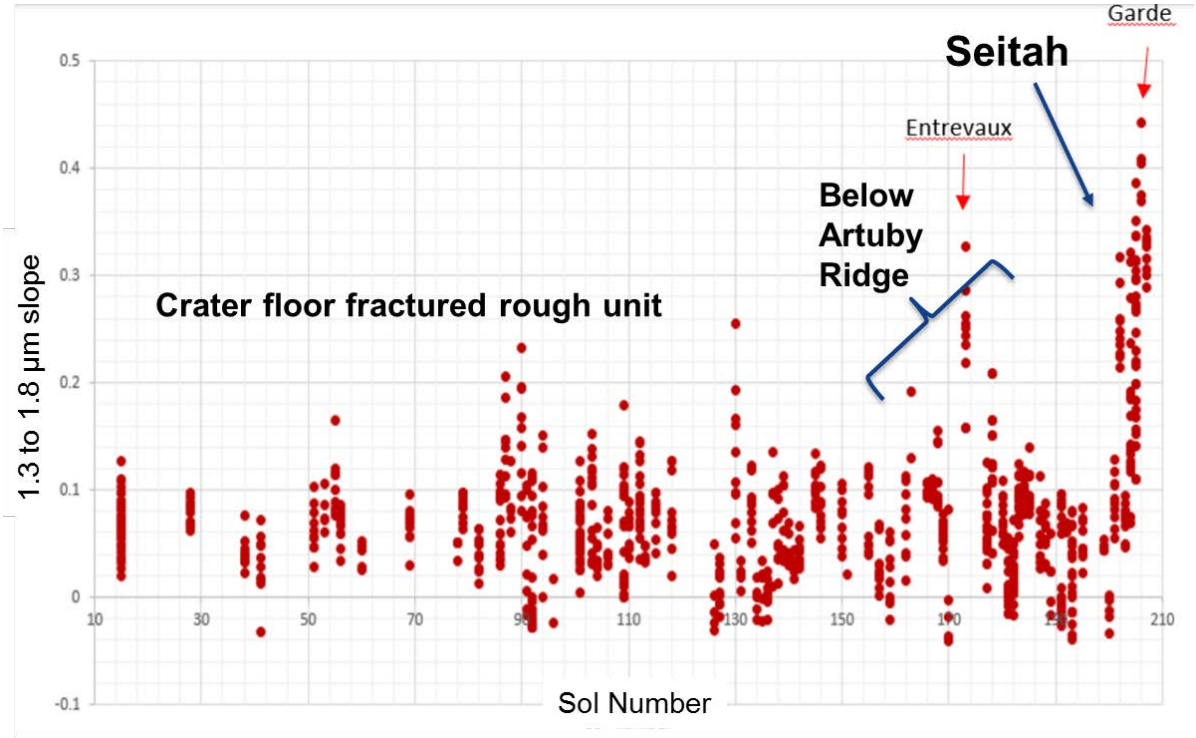

Figure 5.- Slope values in the 1.3-1.8 µm range of VISIR spectra collected until Sol 208

LIBS observations agree with VISIR data. Figure 6 shows the elemental abundances of Seitah rocks to be in the olivine range of the pyroxene-olivine diagram. Comparing the distribution of the rocks in the Cf-fr unit (Figure 3) and Artuby-Seitah (Figure 6), rocks are less felsic and more mafic as the rover traverses from OEB to Seitah. However, there are common rocks in all units, e.g. the rocks showing a distribution in the middle ($0.3<(Mg+Fe)/Si<0.7$) of the pyroxene-olivine diagram.

In contrast with this trend observed in the rocks, the small pebbles on top of the soil show a constant chemical and mineralogical composition. Figure 7 shows the fairly constant concentration of Si, Fe, Mg and Ca in 25 selected points on small pebbles distributed from Sol 72 until sol 236. The pebbles are composed of the same mixture of four minerals, albite, anorthite, diopside and olivine with slight differences in their relative amounts, with olivine as the most abundant (nearly 75%) of the mineral phases.

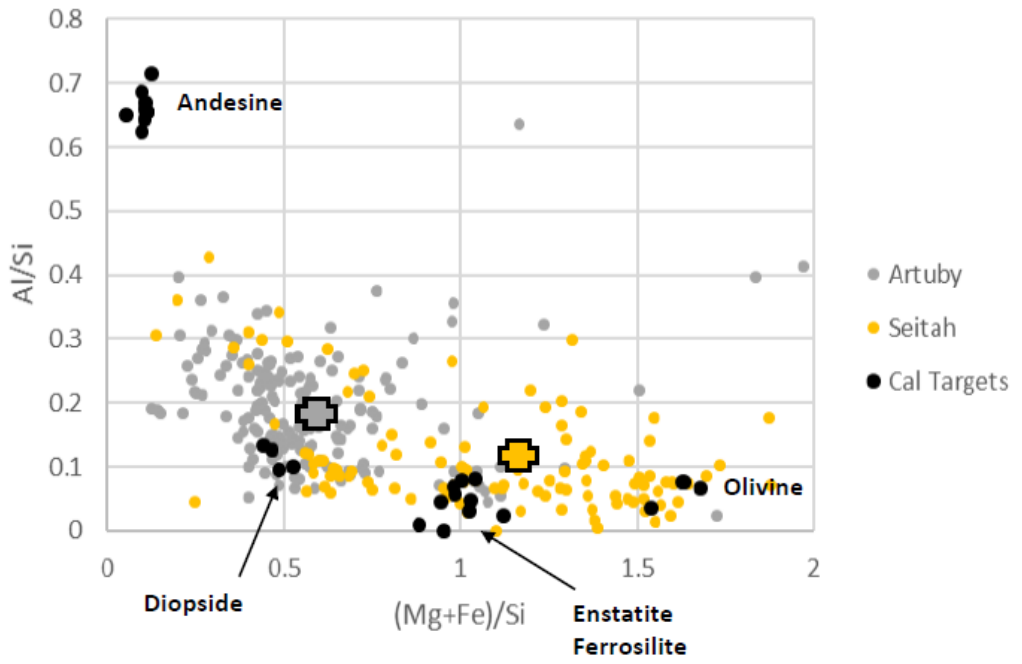

Figure 6.- Diversity of the Artuby and Seitah rocks in comparison with the pyroxene-olivine standards included in the calibration target of SuperCam. Crosses are the mean values for both regions.

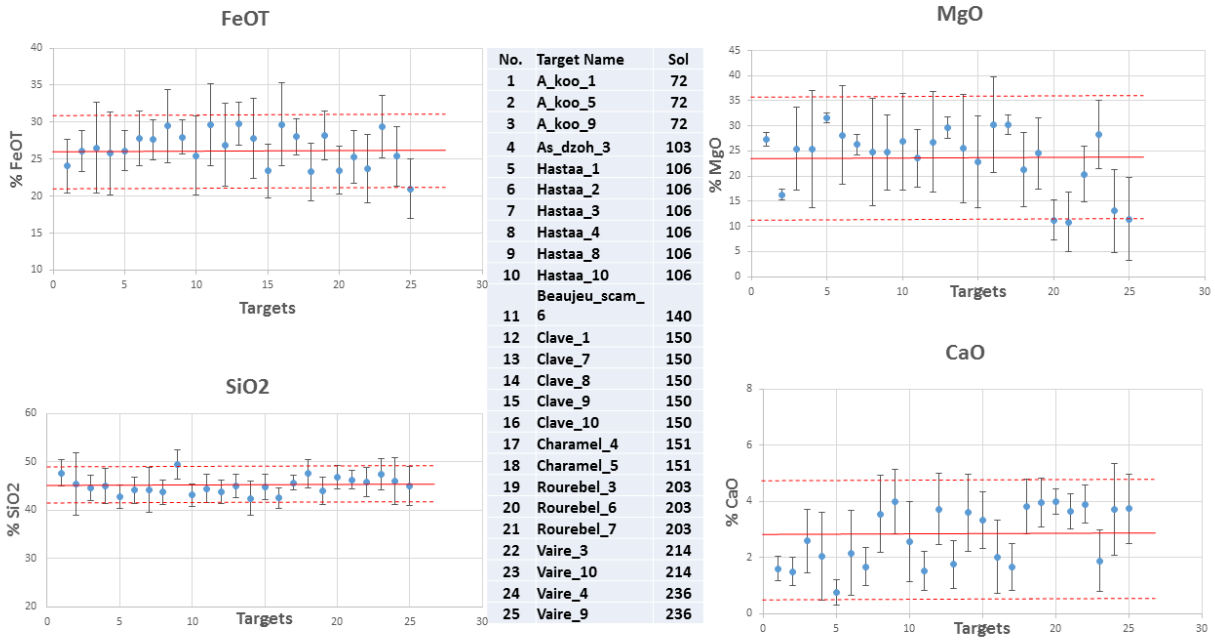

No.	Target Name	Sol
1	A_koo_1	72
2	A_koo_5	72
3	A_koo_9	72
4	As_dzoh_3	103
5	Hastaa_1	106
6	Hastaa_2	106
7	Hastaa_3	106
8	Hastaa_4	106
9	Hastaa_8	106
10	Hastaa_10	106
11	Beaujeu_scam_6	140
12	Clave_1	150
13	Clave_7	150
14	Clave_8	150
15	Clave_9	150
16	Clave_10	150
17	Charamel_4	151
18	Charamel_5	151
19	Rourebel_3	203
20	Rourebel_6	203
21	Rourebel_7	203
22	Vaire_3	214
23	Vaire_10	214
24	Vaire_4	236
25	Vaire_9	236

Figure 7.- Concentration of Si, Fe, Mg and Ca in 25 small pebbles deposited on top of soil surfaces from Sol 72 until Sol 236. The mean value and the ± 2 standard deviation uncertainty

boundary (dashed lines) cover all observed values. The whole FeOT belongs to olivine, while MgOH is split into olivine and diopside, and CaO into anorthite and diopside

CONCLUSIONS

Comparisons to (igneous) Martian meteorites are potentially useful, e.g. [3], to explain the presence of several minerals, although most Martian meteorites are pyroxene- and olivine-rich, e.g., more mafic than the rocks at the landing site but more similar to the rocks in Seitah. In summary, the bedrocks at Octavia Butler landing site and the Cf-fr unit can be interpreted as showing evidence for relatively coarse-grained weathered pyroxenes, iron and titanium oxides and feldspars, while the local soil contains pebbles from a different source (richer in MgO) incorporating olivine grains. Artuby can be considered a transition between Seitah and the Cf-fr units because the presence of olivine in the rocks increases and feldspar-plagioclase minerals decrease. The rocks in Seitah are rich in olivine, decreasing the relative amount of pyroxene and alumino-silicate phases. It is notheworthy that the small pebbles on top of the soils of Seitah and Cf-Fr units have nearly the same composition as Seitah rocks, with olivine in the range of 64-88%, pyroxene between 5 and 15% and feldspar-plagioclase in the range 14-21%.

References

[1] Mandon et al. 2021 Fall AGU, New Orleans, LA, 13-17 Dec.
[2] Beyssac et al. 2021 Fall AGU, New Orleans, LA, 13-17 Dec.
[3] Garcia-Florentino et al. (2021), Talanta, **224**, 121863.